© 2017. Published by The Company of Biologists Ltd | Development (2017) 144, 3698-3705 doi:10.1242/dev.146290

Three-dimensional automated reporter quantification (3D-ARQ) technology enables quantitative screening in retinal organoids

M. Natalia Vergara*,‡, Miguel Flores-Bellver*, Silvia Aparicio-Domingo*, Minda McNally, Karl J. Wahlin§, Meera T. Saxena, Jeff S. Mumm and M. Valeria Canto-Soler*,‡

ABSTRACT

The advent of stem cell-derived retinal organoids has brought forth unprecedented opportunities for developmental and physiological studies, while presenting new therapeutic promise for retinal degenerative diseases. From a translational perspective, organoid systems provide exciting new prospects for drug discovery, offering the possibility to perform compound screening in a three-dimensional (3D) human tissue context that resembles the native histoarchitecture and to some extent recapitulates cellular interactions. However, inherent variability issues and a general lack of robust quantitative technologies for analyzing organoids on a large scale pose severe limitations for their use in translational applications. To address this need, we have developed a screening platform that enables accurate quantification of fluorescent reporters in complex human iPSC-derived retinal organoids. This platform incorporates a fluorescence microplate reader that allows *xyz*-dimensional detection and fine-tuned wavelength selection. We have established optimal parameters for fluorescent reporter signal detection, devised methods to compensate for organoid size variability, evaluated performance and sensitivity parameters, and validated this technology for functional applications.

KEY WORDS: Retinal organoids, Screening, Fluorescence reporter quantification, 3D-ARQ, Human

INTRODUCTION

The last decade has seen a surge in the development of stem cell-based models and technologies, and for good reason, since these systems have opened up numerous opportunities for basic research and clinical applications (Canto-Soler et al., 2016; Fatehullah et al., 2016; Hynds and Giangreco, 2013; Wright et al., 2014; Xinaris et al., 2015; Yin et al., 2016). At the forefront of these efforts is the generation of three-dimensional (3D), stem cell-derived organoid systems. These systems largely resemble the native tissue architecture and recapitulate, to a certain extent, the cellular interactions crucial to the development and function of their *in vivo* counterparts. Therefore, organoids promise not only to be of great value in the translational arena but also to increase our understanding of human development, physiology and disease (Fatehullah et al., 2016; Johnson and Hockemeyer, 2015).

From a basic science point of view, the cumulative knowledge of developmental mechanisms has been instrumental in the generation and optimization of organoid systems. The field is now coming full circle, as these organoids earn their place as essential tools that can provide new insights into the processes underlying human embryonic development (Little, 2016). From a translational perspective, their potential to improve drug development paradigms is arguably one of the most exciting applications of organoid systems, and one that is likely to yield significant therapeutic and economic impact. Nonetheless, key challenges remain that prevent researchers from fully realizing the potential of organoid systems. Among these are issues of variability, limited throughput, shortage of robust quantitative assays, and lack of automation.

In order to address these problems, we have developed a versatile, quantitative and readily accessible method for screening complex stem cell-derived retinal organoids that meets the speed, sensitivity and reproducibility metrics required for compound screening applications. This platform, termed 3D automated reporter quantification (3D-ARQ), utilizes a microplate reader featuring highly sensitive *xyz*-dimensional detection and a tunable excitation/emission double monochromator system to facilitate assay optimization and concurrent multiple fluorophore detection. We have optimized and validated this technology using a human induced pluripotent stem cell (iPSC)-derived retinal organoid model developed in our laboratory that recapitulates essential hallmarks of human eye development (Zhong et al., 2014). With this model we provide proof-of-principle data regarding the applicability of 3D-ARQ technology for quantitative analysis of the dynamics of developmental processes and cellular physiological states.

RESULTS

Parameter optimization for fluorescent reporter quantification in retinal organoids

We previously established a protocol for the efficient and reproducible generation of retinal organoids from human iPSCs (Zhong et al., 2014). These organoids consist of a fully laminated neural retina and a small amount of retinal pigmented epithelium (RPE) bundled at the edge of the tissue. Moreover, the timing of retinal organoid differentiation closely mimics that of the developing human retina *in vivo*. To take full advantage of this model, quantitative analytical methods are needed that can easily be applied in smaller research labs yet still exhibit a level of robustness, sensitivity and speed that could allow for larger scale applications. Considering the amenability of stem cell lines harboring fluorescent reporters for multiple applications and realizing that many physiological assays are fluorescence based, we have developed a

The Wilmer Eye Institute, Johns Hopkins University School of Medicine, Baltimore, MD 21287, USA.

*Present address: CellSight – Ocular Stem Cell and Regeneration Research Program, Department of Ophthalmology, School of Medicine, University of Colorado, Anschutz Medical Campus, Aurora, CO 80045, USA. §Present address: Shiley Eye Institute, University of California San Diego, La Jolla, CA 92093, USA.

‡Authors for correspondence (natalia.vergara@ucdenver.edu; valeria.canto-soler@ucdenver.edu)

M.N.V., 0000-0003-4545-8181; J.S.M., 0000-0002-2575-287X; M.V.C.-S., 0000-0001-8692-034X

Received 28 October 2016; Accepted 30 August 2017

Development (2017) 144, 3698-3705 doi:10.1242/dev.146290

microplate reader approach for rapidly and accurately quantifying relative fluorescence reporter intensity levels in organoid model systems.

The plate reader of choice needed to provide specific functionalities required for 3D organoid-based assays, while allowing enough flexibility for use with a variety of plate formats and applications. The TECAN Infinite M1000 met these specifications, namely: (1) the option of a top read mode that allows the use of black v-bottom plates, maximizing fluorescence acquisition and diminishing light scattering and interference; (2) the ability to focus in the *z*-dimension, a crucial feature when assaying 3D models; (3) the capacity to carry out regionally demarcated scans in the *xy* plane; (4) adjustable wavelength selection (230 to 850 nm) and spectral scans using excitation/emission double monochromators. Importantly, this system has been previously validated for use in whole-organism large-scale screening assays using zebrafish larvae (Walker et al., 2012; Wang et al., 2015; White et al., 2016).

To establish optimal conditions for quantifying reporter levels in organoids we generated a transgenic human iPSC line constitutively expressing a green fluorescent protein (GFP) reporter. The parameters tested included: plate type, well shape, volume, and instrument settings such as flash mode and number of flashes. The results are summarized in Tables S1 and S2. All following experiments were performed using optimized settings and black v-bottom 96-well plates, which enable self-centering and thus reproducible localization of retinal organoids.

An important consideration when designing fluorescence-based assays is the potential interference from background autofluorescence that could result in decreased sensitivity, i.e. lower signal-to-background (S:B) ratios (see Table S3). Thus, we evaluated the autofluorescence profiles of wild-type retinal organoids with or without RPE tissue, under live or fixed conditions, compared with medium alone. Clear medium was used in all assays as the presence of Phenol Red resulted in high background levels. We performed emission wavelength scans (up to 700 nm), using excitation wavelengths of common fluorophores spanning a range of reporter 'colors' (blue to far red; Fig. S1). We concluded that retinal organoids do not contribute significantly to autofluorescence background profiles at any of the wavelengths tested. Accordingly, any background signals observed can be attributed primarily to the medium or multiwell plate. Shorter excitation wavelengths yielded the highest levels of background, suggesting that fluorophores of longer excitation wavelengths (>500 nm, i.e. from yellow to far red) would be ideal for minimizing background interference. Also, paraformaldehyde fixation did not result in increased background signals. This facilitates additional flexibility in terms of the types of applications that can be pursued with this system, such as whole-mount immunofluorescence or fluorescence *in situ* hybridization (FISH). Importantly, the presence of RPE in retinal organoids also did not result in increased autofluorescence.

Sensitivity, reproducibility and variability assessment

Next, we determined optimal wavelength parameters for various fluorophores by performing excitation and emission scans on stained or transgenic retinal organoids (Fig. S2), and used these parameters to assess the sensitivity, technical reproducibility and sample variability of this technology. Retinal organoids were stained with: (1) Hoechst, a blue fluorescent DNA-intercalating dye; (2) Calcein AM, a green fluorescent cell-permeant dye that accumulates in the cytoplasm of live cells and is commonly used in viability assays; (3) DiI, a red fluorescent lipophilic dye that is retained in cell membranes and used for cell-tracing experiments; and (4) Bodipy TR methyl ester, a longer wavelength red fluorescent dye that permeates cell membranes, staining mitochondria and endomembranous organelles, and is used for cell tracking. We also included in this analysis transgenic retinal organoids expressing cytoplasmic GFP or membrane-tagged yellow fluorescent protein (YFP).

Data from six independent scans on fluorescently labeled or transgenic retinal organoids demonstrated a range of sensitivities, with S:B ratios above 2-fold, and a high level of technical reproducibility across scans within each sample [Fig. 1; coefficient of variation (%CV) <15% in all cases; Table S3]. However, a higher degree of individual variability was observed across organoids expressing the same fluorophore (see the differences in S:B ratio for each sample). These differences might not compromise the statistical significance of assays involving high-intensity fluorophores and/or high expression levels, but might become problematic at low fluorescence intensities. Thus, we set out to devise ways to address this potential limitation.

Size normalization and quantitative capacity

Owing to inherent characteristics of our retinal organoid model, we reasoned that a major source of variability in this system might be organoid size. To circumvent this, a second, globally expressed transgene or ubiquitous counterstaining could be used to normalize the fluorescence intensity outputs of a complementary experimental reporter, providing a means to control for differences in size across organoids. This 'ratiometric' reporter-based assay strategy has been applied effectively in cell culture high-throughput screening (Michael et al., 2008). To test whether this approach can account for size variation, we double-stained retinal organoids of different sizes with fixed concentrations of Bodipy TR and Calcein AM and used the ratio between the fluorescence readouts of both fluorophores for normalizing for size differences. The data show that this strategy reduces the degree of variability observed, as compared with using a single experimental reporter (Fig. 2A-C). Moreover, when testing retinal organoids of a range of sizes, we found a linear correlation between the fluorescence intensity readouts for both fluorophores, further verifying the robustly quantitative nature of the approach (Fig. 2D).

To verify that the fluorescence measures indeed correlate with organoid size, we compared the fluorescence intensity of retinal organoids stained with Bodipy TR with their estimated volume, as calculated from the surface area of their flat projection, and again found a linear correlation (Fig. 2E). Finally, we performed serial dilutions of Bodipy TR, using a fixed concentration of Calcein AM for counterstaining. The significant reduction in variability for each group of samples (Fig. 2F,G) and the improved R^2 values after normalization demonstrate the power of this approach (R^2=0.8557 and 0.9999 before and after normalization, respectively) and illustrate the wide dynamic range capacity of the technology.

Application to the quantification of transgene expression levels

In order to exemplify the utility of 3D-ARQ for accurately quantifying transgenic fluorescent reporter expression, we generated chimeric retinal organoids that express membrane-tagged YFP (m-YFP) in ∼45% of the cells, and compared them with wild-type (non-transgenic) and transgenic retinal organoids expressing YFP ubiquitously (Fig. 3A-C). Bodipy TR counterstaining was used for size normalization. The results

Development (2017) 144, 3698-3705 doi:10.1242/dev.146290

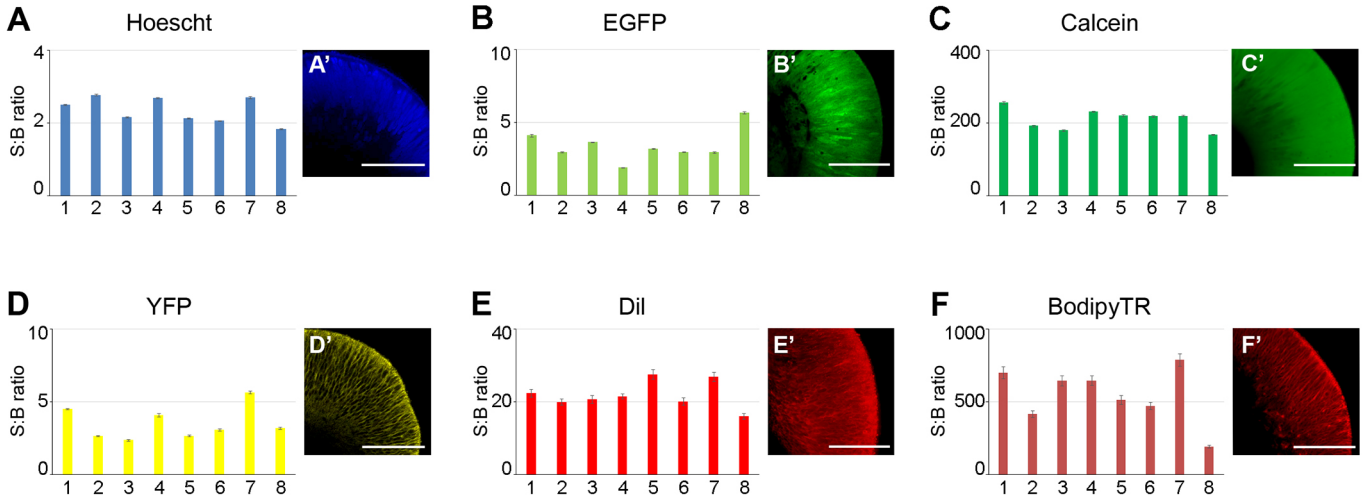

Fig. 1. Sensitivity and reproducibility of signal detection. (A-F) Signal-to-background (S:B) ratios of live retinal organoids at 5 weeks of differentiation, stained with different fluorescent dyes or expressing fluorescent reporters as indicated. Each bar corresponds to an individual organoid. Six independent measurements per organoid per condition were performed within a 2 h period to assess technical reproducibility. Error bars represent s.e.m. of technical replicates. (A′-F′) Confocal images of whole-mount organoids representative of each condition, showing the subcellular distribution of fluorophores. Scale bars: 100 µm.

demonstrate that the system possesses the level of sensitivity necessary to discern such differences in fluorescent reporter expression (Fig. 3D).

To further validate the quantitative power of 3D-ARQ, we generated m-YFP chimeric organoids at random proportions, determined their fluorescence intensities using Bodipy TR for normalization, and then dissociated them into single cells and used flow cytometry to assess the percentage of YFP^+ cells in individual organoids. Fig. 3E shows a linear correlation between these two measurements.

Quantitative measurements of developmental progression

As previously described, our retinal organoid model mimics the major events of human retinal development both spatially and temporally. Thus, we used this model to assess the ability of 3D-ARQ to quantitatively track the progression of developmental processes, such as cellular differentiation. We performed whole-mount immunohistochemistry for Pou4f2 (also known as Brn3b), which is expressed in retinal ganglion cell (RGC) precursors as they are born and during differentiation, using Alexa Fluor 546 for fluorescent detection (Fig. 4A-E). Sytox Green staining was used for size normalization within each differentiation time point. Notably, we were able to detect differences in fluorescent signal at the time points tested (weeks 5-9), and the incremental values observed were well correlated with the wave of generation of RGC precursors in developing retinal organoids, as observed in both the current experiments and those from our previous work (Zhong et al., 2014). The same was true for the expression pattern of Otx2, which

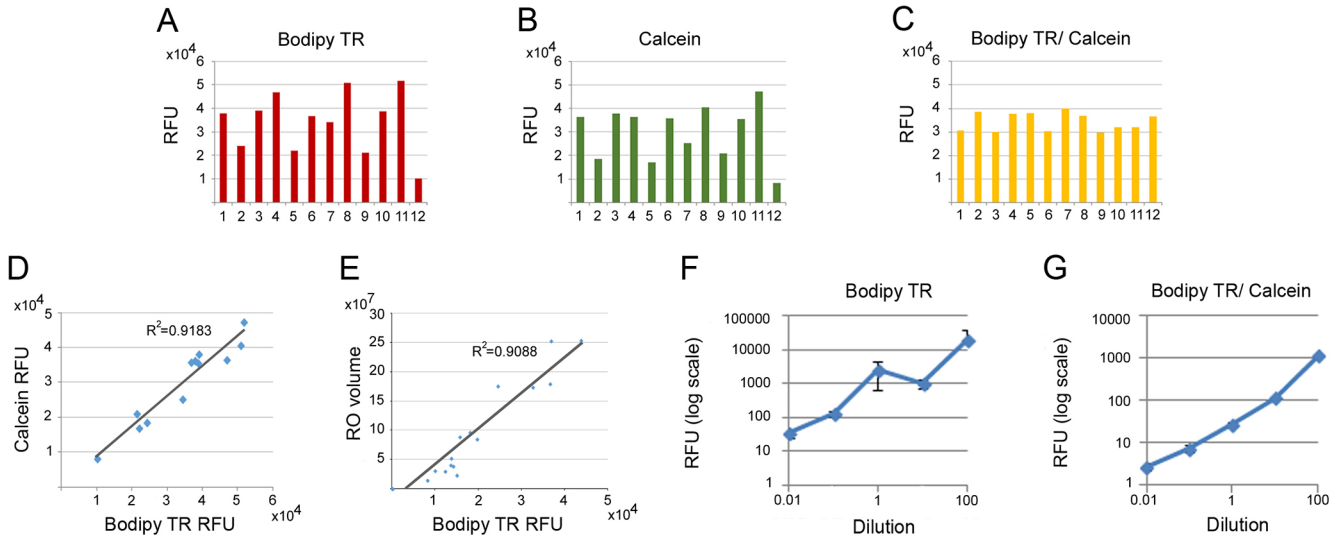

Fig. 2. Normalization of fluorescence intensity using a globally expressed fluorophore. (A-D) Live retinal organoids at 5 weeks of differentiation were double stained with Bodipy TR and Calcein AM. Fluorescence intensity readouts are shown for 12 individual organoids for each fluorophore (A,B), and their Bodipy TR values after Calcein AM normalization (C). The correlation between the fluorescence values for both fluorophores is shown in D. (E) The correlation between fluorescence intensity of Bodipy TR-stained retinal organoids (RO) and their volume (n=16). (F,G) Five-week retinal organoids were treated with serial dilutions of Bodipy TR and counterstained with a fixed concentration of Calcein AM. Mean fluorescence is shown for Bodipy TR staining before (F) and after (G) normalization. Error bars represent s.e.m. for three biological replicates per dilution. RFU, relative fluorescence units.

Development (2017) 144, 3698-3705 doi:10.1242/dev.146290

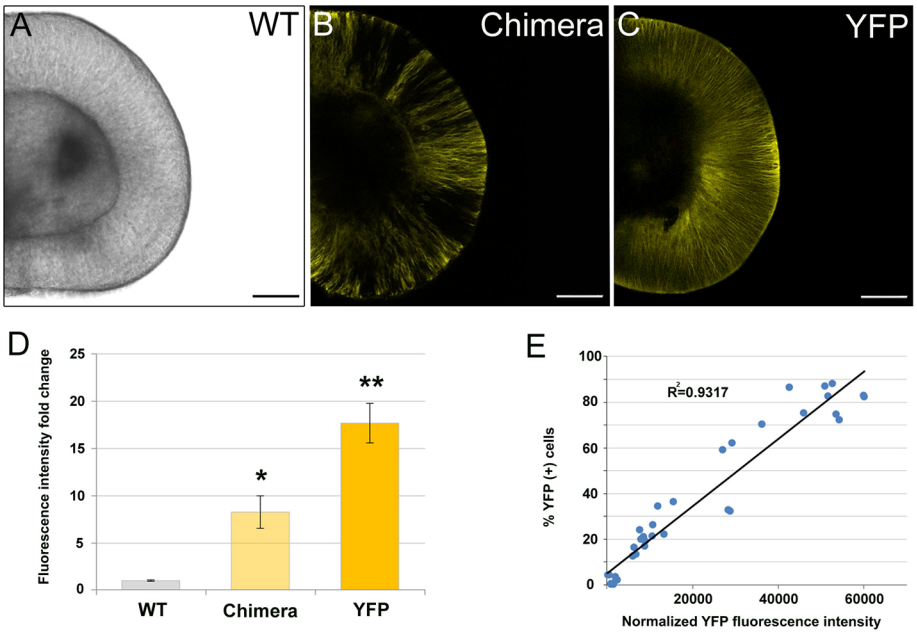

Fig. 3. Quantification of transgene expression levels. (A-C) Confocal images of live retinal organoids at 5 weeks of differentiation comparing (A) wild-type (non-transgenic; WT), (B) chimeric (wild-type/m-YFP) and (C) global m-YFP transgenic organoids. Scale bars: 100 µm. (D) Fold change in m-YFP fluorescence intensity measured for each condition and normalized using Bodipy TR counterstaining. Chimeric organoids generated at a 45% YFP ratio were used in this experiment. Error bars represent s.e.m. of five biological replicates per condition. $^{**}P<0.01$, $^{*}P<0.05$, by two-tailed Student's *t*-test with unequal variance. (E) The YFP fluorescence intensity of randomly generated chimeric organoids was evaluated using 3D-ARQ normalized to Bodipy TR counterstaining, and compared with the percentage of YFP^{+} cells in individual organoids by flow cytometry analysis after dissociation (n=20).

is expressed in photoreceptor precursors, when evaluated between weeks 5 and 11 of differentiation, using Alexa Fluor 514 for fluorescence detection and Bodipy TR counterstaining (Fig. 4F-J).

These experiments also illustrate the power of the technology to detect changes in both the inner and outer layers of the retinal organoids at various time points during the process of cell differentiation and lamination.

Application to the quantification of changes in physiological state

We next tested the ability of the 3D-ARQ system to evaluate the physiological status of cells within the organoids. Oxidative stress is at the basis of the pathophysiology of many chronic diseases, including those affecting the retina (Athanasiou et al., 2013; Cano et al., 2010; Hollyfield et al., 2008; Jarrett and Boulton, 2012; Kowluru and Chan, 2007; Masuda et al., 2017; Nita and Grzybowski, 2016; Nishimura et al., 2017; and references therein). We assessed the capacity of this system to quantitatively measure the accumulation of reactive oxygen species (ROS) following an oxidative insult, as a relevant example of a potential application for therapeutic screening.

Retinal organoids were treated for 3 h with increasing concentrations of hydrogen peroxide, and ROS production was detected using dihydroethidium (DHE), a superoxide indicator that, upon oxidation in the cytosol, intercalates with DNA and emits a bright red fluorescence (emission peak of 606 nm). Once again, we were able to measure substantial differences in fluorescence intensity among all conditions (Fig. 5A).

Finally, we tested the capacity of this technology to detect physiological changes in retinal organoids at advanced stages of differentiation. For this purpose we devised an assay based on the membrane-permeant dye JC-1, which is widely used to monitor mitochondrial membrane potential (thus providing a measure of mitochondrial health). JC-1 dye exhibits membrane potential-dependent accumulation in mitochondria: in normal circumstances the dye forms aggregates in the mitochondrial membrane, emitting red fluorescence (~590 nm); however, upon membrane depolarization it shifts to its monomeric form, fluorescing in the green part of the spectrum (~529 nm). Consequently, a decrease in the red/green fluorescence intensity ratio indicates a decrease in mitochondrial membrane potential, which results in a disruption in the respiratory electron transport chain.

For this assay we used retinal organoids at 87 weeks of differentiation. It has previously been reported that after 6 months of differentiation, photoreceptors in retinal organoids have achieved a relatively advanced degree of maturation, including well-developed inner segments (Wahlin et al., 2017; Zhong et al., 2014). We reasoned that since mitochondria are highly concentrated in the inner segment of photoreceptor cells, the majority of the JC-1 staining would be representative of cells localized in the outer nuclear layer. Moreover, mitochondrial staining dyes, including JC-1, have previously been used to preferentially label photoreceptor cells both in retinal explants and in primary retinal cultures (Bianchini et al., 2008; Kuse et al., 2014; Panfoli et al., 2009; Pearson et al., 2016; Rajendram et al., 2007; Roehlecke et al., 2011). As expected, confocal imaging of live retinal organoids stained with JC-1 revealed a high concentration of both red and green fluorescence in the outer layer of the organoids, in structures that are likely to correspond to the photoreceptor inner segments (Fig. 5B-C′). Additionally, immunostaining for recoverin, a photoreceptor-specific calcium-binding protein, provided further evidence of the photoreceptor nature of the cells that display JC-1 staining (Fig. 5B, inset).

We performed a longitudinal quantitative analysis in live retinal organoids by assessing the initial red/green fluorescence intensity ratio of JC-1-stained organoids using 3D-ARQ, followed by subdivision into treatment and control groups; the treatment group was incubated with the protonophore carbonyl cyanide m-chlorophenyl hydrazone (CCCP) (10 µM), a mitochondrial uncoupler, whereas the control group was exposed to vehicle alone (0.01% DMSO). A marked decrease in the JC-1 aggregate/monomer fluorescence ratio was observed in CCCP-treated organoids after 6, 24 and 48 h of treatment (Fig. 5D). When the protonophore was removed and the organoids were left to recover in their normal medium for 3 days and re-evaluated, the JC-1 ratio in the treated group was indistinguishable from that of the controls.

Development (2017) 144, 3698-3705 doi:10.1242/dev.146290

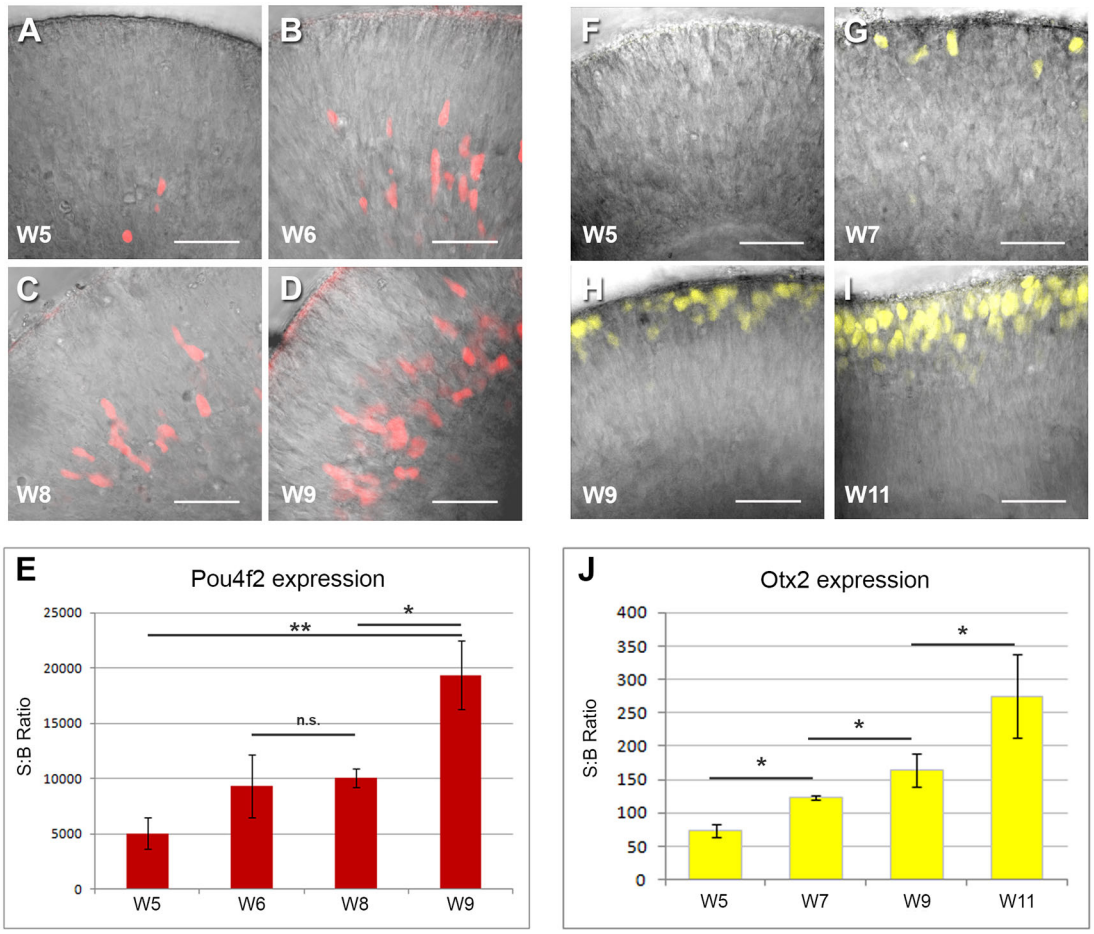

Fig. 4. Assessment of developmental progression of gene expression. (A-D) Confocal images of fixed whole-mount retinal organoids immunostained for Pou4f2 at various differentiation time points [weeks (W) 5-9]. (E) Mean S:B ratios for Pou4f2 immunofluorescence at each time point, normalized to Sytox Green staining. (F-I) Confocal images of fixed whole-mount retinal organoids immunostained for Otx2 at weeks 5-11 of differentiation. (J) Mean S:B ratios for Otx2 immunofluorescence at each time point, normalized to Bodipy TR staining. Error bars represent s.e.m. of five biological replicates per time point; **P*<0.05, ***P*<0.01, by two-tailed Student's *t*-test with unequal variance; n.s., not significant. Scale bars: 100 µm.

These results provide proof of principle supporting the utility of 3D-ARQ in longitudinal studies performed in live organoids at late differentiation stages.

DISCUSSION

The advent of stem cell-based 3D organoid systems has opened up new opportunities to improve drug development paradigms. This comes at a time when drug discovery is at a crossroads: technological advances have increased the speed and lowered the costs of lead compound identification, but when taken to clinical trials 90% of these compounds fail to progress through phase I, resulting in billions of dollars in economic losses and delays in the development of much-needed therapeutic agents (Hynds and Giangreco, 2013; Paul et al., 2010; Ranga et al., 2014). This discrepancy can be attributed, at least in part, to a reliance on drug discovery platforms involving simplified 2D culture systems that do not adequately recapitulate *in vivo* cellular context and physiology. In this scenario, human stem cell-derived organoids have the potential to bridge the gap between primary compound screening, costly animal studies, and human trials, as they provide a more physiologically relevant, human-based context, while allowing the necessary flexibility and level of control of an *in vitro* system (Fatehullah et al., 2016; Hynds and Giangreco, 2013; Ranga et al., 2014). However, there is currently a lack of quantitative technologies that can facilitate the application of 3D organoids to drug screening.

To aid in this pursuit, we have developed and optimized a versatile platform that enables fluorescence-based quantitative measurements in complex, 3D retinal organoids. In order to illustrate the versatility of the system for a variety of applications, we chose to incorporate throughout these studies multiple fluorophores exhibiting different spectral characteristics and subcellular distributions, including dyes and transgenic proteins. However, when designing a fluorescence-based assay it is important to be mindful that sensitivity is dependent not only on the capabilities of the instrument and the biological system's background, but also on the characteristics of the fluorescent reporter/dye; for example, the concentration of the fluorophore (i.e. the number of expressing or labeled cells and the intracellular concentration), the quantum yield (the number of fluorescence photons emitted per excitation photon absorbed) and its extinction coefficient (its capacity to absorb light at a specific wavelength) (Lichtman and Conchello, 2005). Therefore, even though shorter wavelength reporters may not perform ideally in terms of background, this limitation can be overcome with the use of bright or highly expressed reporters.

The 3D-ARQ platform presented here performs well in smaller laboratory settings, where its quantitative capacity might prove

Development (2017) 144, 3698-3705 doi:10.1242/dev.146290

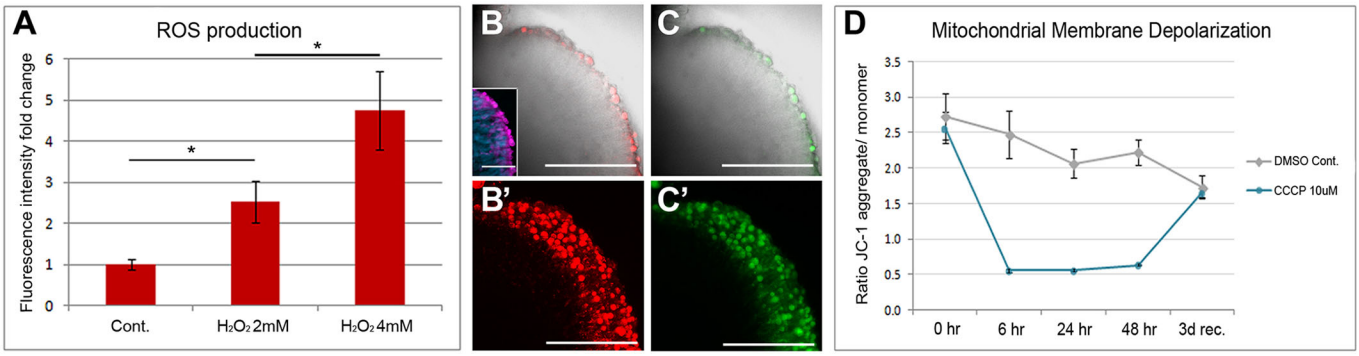

Fig. 5. Assessment of the physiological status of retinal organoids. (A) Live retinal organoids at 5 weeks of differentiation were treated with 0 (Cont.), 2 and 4 mM H_2O_2, and stained with DHE to measure ROS production. Shown is the mean fluorescence intensity fold change among conditions. *n*=5 biological replicates per condition. Error bars represent s.e.m. **P*<0.05, by two-tailed Student's *t*-test with equal variance. (B-C′) Confocal imaging of live retinal organoids at 87 weeks of differentiation stained with JC-1 dye. Red fluorescence, representing JC-1 aggregates (B,B′), and green fluorescence, representing the monomeric form of the dye (C,C′), were concentrated in cells in the outer layer of the organoids. B′ and C′ are confocal *z*-stack reconstructions corresponding to the organoids shown in B and C. Scale bars: 100 µm. Inset in B shows recoverin immunolabeling (magenta) in the outer surface of the neural retina, with DAPI-stained nuclei in blue. Scale bar: 50 µm. (D) Mitochondrial membrane depolarization in live retinal organoids at 87 weeks of differentiation was assessed by JC-1 staining. After measuring initial JC-1 aggregate/monomer ratios, organoids were treated with 10 µM CCCP or DMSO, and re-evaluated at 6, 24 and 48 h, and once again after a 3-day recovery period. *n*=4 organoids per group. Error bars represent s.e.m.

useful for developmental or physiological basic science studies. Yet, the estimated daily capacity of the instrument exceeds 200,000 samples per day, while also meeting the requirements of sensitivity, reproducibility and the possibility for automation that afford it the potential for future large-scale screening applications, once the conditions for organoid generation and handling are optimized.

The remaining challenge is now to increase the throughput in organoid generation, which is admittedly a laborious process and likely to be the limiting factor for increasing assay scale. Another important hurdle is the variability of the retinal organoid system itself. From our experience using our previously published protocol (Zhong et al., 2014), we have found that the greatest source of variability in this system at each particular differentiation time is organoid size. Some variability in cellular composition exists at each time point, but to a lesser degree, as exemplified by the spread of the normalized values for both Otx2 and Pou4f2 at each developmental time tested (Fig. 4; the fluorescence micrographs in this figure illustrate typical examples of the expression patterns of these proteins that we observe in retinal organoids). We have proposed and validated one possible strategy to normalize for differences in organoid size by applying a ratiometric approach based on a second, globally expressed fluorophore (Fig. 2). An important consideration when designing ratiometric assays is to choose a fluorophore combination with enough spectral separation to maximize signal discrimination. Fluorophores with large Stokes shifts and narrow spectral bandwidths are particularly useful in this respect (Lichtman and Conchello, 2005). Alternatively, organoids could be sorted by size prior to screening, taking advantage of existing automated sorting technologies designed for use with large particles, cell clumps, or even small organisms, such as the Complex Object Parametric Analyzer and Sorter (COPAS, Union Biometrica). Moreover, this type of technology, once optimized for organoid sorting, could also facilitate their transfer to 96-well plates, improving the speed of the overall process for drug screening applications.

Ultimately, the best strategy to use will be largely dependent on the question being asked and the particular experimental design. For example, performing longitudinal analyses of fluorescence intensities in individual organoids over time or before and after treatment, as would be the case if they were used in drug screening, would minimize the problem of inter-organoid cellular heterogeneity. Thereby, any changes in reporter expression after treatment would be highlighted by normalizing to pretreatment values for each individual organoid (Walker et al., 2012). Here, we have provided proof of principle of the utility of this approach in longitudinal studies on live retinal organoids at very late stages of differentiation (Fig. 5D). This strategy would be particularly well suited for experiments on organoids expressing transgenic fluorescent reporters, and for adapting the technology to other organoid systems.

In conclusion, we believe that 3D-ARQ technology will broaden the applicability of retinal organoid systems (and possibly others) for basic research as well as translational applications, including studies of development, physiological and disease mechanisms, drug screening and toxicology.

MATERIALS AND METHODS

Human iPSC lines and retinal differentiation

A human episomal iPSC line derived from $CD34^+$ cord blood was used in this study (A18945, ThermoFisher Scientific; Burridge et al., 2011). m-YFP and GFP-expressing transgenic lines were generated from this line as described in the supplementary Materials and Methods. All cell lines were routinely tested for *Mycoplasma* contamination by PCR. Cell culture, retinal differentiation and organoid formation were conducted as previously described (Zhong et al., 2014). Retinal organoids at 5 weeks of differentiation were used for experiments, unless otherwise indicated. At the time of analysis, individual organoids were transferred to single wells of black v-bottom 96-well plates (Greiner).

Staining with fluorescent dyes and immunofluorescence

Organoids were rinsed in clear retinal differentiation medium (cRDM; supplementary Materials and Methods), and incubated at 37°C for 90 min in the corresponding dye solutions diluted in cRDM, followed by three washes in cRDM (*n*=8 organoids per condition). For whole-mount immunofluorescence, retinal organoids at various differentiation stages were fixed in 4% paraformaldehyde for 10 min and labeled using rabbit anti-Otx2 antibody (Millipore, AB9566; Zhong et al., 2014) or goat anti-Brn3b (Pou4f2) antibody (Santa Cruz Biotechnologies, SC-6026x), followed by incubation with goat anti-rabbit Alexa Fluor 514 (ThermoFisher Scientific, A-31558) or donkey anti-goat Alexa Fluor 546 (ThermoFisher Scientific, A-11056), and counterstained with Bodipy TR or Sytox Green, respectively (*n*=5 per time point). Organoids were plated individually in black v-bottom 96-well plates for fluorescence scanning. For reproducibility testing, six

Development (2017) 144, 3698-3705 doi:10.1242/dev.146290

independent scans were performed on the same plates within 2 h. Subsequently, confocal imaging was performed on whole organoids using an Olympus FV1000 microscope. For size calculation, organoids were imaged using a stereomicroscope with an Infinity 3S-1UR CCD camera (Lumenera), and ImageJ (NIH) was used to measure the surface area of the flat projection, from which the volume was approximated as a sphere. For immunofluorescence on sections, organoids were fixed in 4% paraformaldehyde, embedded in sucrose:OCT (Fisher HealthCare, 4585), cryosectioned at 12 µm thickness, and labeled using rabbit anti-recoverin antibody (Millipore-ThermoFisher Scientific, AB5585). For further details on dye staining and immunofluorescence, see the supplementary Materials and Methods.

Flow cytometry

Chimeric retinal organoids were generated by co-culturing wild-type and m-YFP-expressing human iPSC lines (generated as described in the supplementary Materials and Methods) in various proportions, and following the cell culture and organoid differentiation protocol previously described (Zhong et al., 2014). Fluorescence intensity in live organoids was determined using the TECAN microplate reader after Bodipy TR counterstaining (n=20). Organoids were then individually dissociated using the Minute Single Cell Isolation Kit (Invent Biotechnologies, SC-012), resuspended in PBS, and analyzed using an Accuri C6 flow cytometer (BD Biosciences). Data analysis was performed using Accuri C6 software (BD Biosciences), and fluorescence cutoff values were determined by comparing the fluorescence histograms generated from wild-type versus global YFP-expressing dissociated organoids.

Fluorescence microplate reader assays

A TECAN Infinite M1000 microplate reader equipped with excitation and emission modules, fluorescence top read module, and i-Control software package was used for all assays. Parameters tested for optimization are described in Table S1, and were obtained by comparing GFP-expressing versus wild-type, non-stained retinal organoids (n=6 each). In all subsequent experiments, organoids were plated individually in polypropylene black v-bottom 96-well plates (Greiner) filled with 340 µl cRDM, and fluorescence intensity readouts were obtained using the optimized settings and the excitation and emission wavelengths described in Fig. S2. For autofluorescence background evaluation, emission scans from 415-700 nm using fixed excitation wavelengths (405, 440, 488, 515, 559 and 635 nm) were performed on live versus fixed retinal organoids and in the presence or absence of RPE (n=5 organoids/condition).

Oxidative stress assay

Organoids were incubated with a 0, 2 or 4 mM H_2O_2 in cRDM at 37°C for 4 h (n=5 per condition) to induce an oxidative insult. After two washes in PBS they were incubated in 5 µM dihydroethidium (DHE; ThermoFisher Scientific) in cRDM for 50 min at 37°C, rinsed once in cRDM and plated individually in 96-well plates for fluorescence scanning (excitation wavelength/bandwidth, 498/5 nm; emission wavelength/bandwidth, 590/10 nm).

Mitochondrial membrane depolarization assay

Retinal organoids at 87 weeks of differentiation were plated in black v-bottom 96-well plates containing cRDM, and baseline background fluorescence was measured using the TECAN microplate reader with 535/17 nm excitation and 590/17 nm emission wavelength/bandwidth for red; and 485/11 nm excitation and 530/15 nm emission wavelength/bandwidth for green. Organoids were then transferred to 35-mm culture dishes and incubated in 4.5 µM JC-1 (ThermoFisher Scientific, T3168) in long-term culture medium (see supplementary Materials and Methods) for 30 min at 37°C. They were then washed twice in PBS and replated in black v-bottom 96-well plates for fluorescence reading using the same parameters and a fixed gain value. Subsequently, organoids were divided into a treatment group incubated with 10 µM carbonyl cyanide m-chlorophenyl hydrazone (CCCP; Sigma-Aldrich, C2759), and a control (DMSO) group (n=4 organoids/group). Fluorescence intensity was remeasured after 6, 24 and 48 h of treatment, with JC-1 added to the medium during the last 30 min of incubation. After 48 h, mitochondrial stressor was removed and the organoids were allowed to recover in long-term culture medium for 3 days, at which point JC-1 incubation and fluorescence measurements were repeated.

Data analysis and statistics

Background subtraction was performed on raw fluorescence intensity data using the corresponding value of cRDM alone for all conditions. Size normalization for a global fluorophore was performed using Eqn S1 in the supplementary Materials and Methods. Equations for determining assay quality are shown in Table S3 and as previously described (Inglese et al., 2007; White et al., 2016; Zhang, 2008, 2011). Grubbs' test was used to identify outliers, and Bartlett's test was used to assess equality of variance. Statistical significance was assessed using Student's t-test for pairwise comparisons.

Acknowledgements

We thank David Ackerly for technical advice on the generation of vectors; Marisol Cano for technical advice on physiological assays; David White for assistance with confocal imaging; and David Kays, Alla Abdelwahab and Christian Hernandez for technical support.

Competing interests

The authors declare no competing or financial interests.

Author contributions

Conceptualization: M.N.V., J.S.M., M.V.C.-S.; Methodology: M.N.V., K.J.W., M.T.S., J.S.M., M.V.C.-S.; Validation: M.N.V.; Formal analysis: M.N.V.; Investigation: M.N.V., M.F.-B., S.A.-D., M.M.; Resources: J.S.M.; Writing - original draft: M.N.V.; Writing - review & editing: M.N.V., M.F.-B., S.A.-D., M.M., K.J.W., M.T.S., J.S.M., M.V.C.-S.; Visualization: M.N.V., M.F.-B., M.V.C.-S.; Supervision: M.V.C.-S.; Project administration: M.N.V.; Funding acquisition: M.V.C.-S.

Funding

This work was supported by National Institutes of Health grants EY022631 (M.V.C.-S.), TR000945 (J.S.M. and M.T.S.) and Core grant EY1765, Dr. Ralph and Marian Falk Medical Research Trust (M.V.C.-S.) and the William & Mary Greve Special Scholar Award from Research to Prevent Blindness (M.V.C.-S.). Deposited in PMC for release after 12 months.

Supplementary information

Supplementary information available online at
http://dev.biologists.org/lookup/doi/10.1242/dev.146290.supplemental

References

Athanasiou, D., Aguilà, M., Bevilacqua, D., Novoselov, S. S., Parfitt, D. A. and Cheetham, M. E. (2013). The cell stress machinery and retinal degeneration. *FEBS Lett.* **587**, 2008-2017.

Bianchini, P., Calzia, D., Ravera, S., Candiano, G., Bachi, A., Morelli, A., Bruschi, M., Pepe, I. M., Diaspro, A. and Panfoli, I. (2008). Live imaging of mammalian retina: rod outer segments are stained by conventional mitochondrial dyes. *J. Biomed. Opt.* **13**, 054017.

Burridge, P. W., Thompson, S., Millrod, M. A., Weinberg, S., Yuan, X., Peters, A., Mahairaki, V., Koliatsos, V. E., Tung, L. and Zambidis, E. T. (2011). A universal system for highly efficient cardiac differentiation of human induced pluripotent stem cells that eliminates interline variability. *PLoS ONE* **6**, e18293.

Cano, M., Thimmalappula, R., Fujihara, M., Nagai, N., Sporn, M., Wang, A. L., Neufeld, A. H., Biswal, S. and Handa, J. T. (2010). Cigarette smoking, oxidative stress, the anti-oxidant response through Nrf2 signaling, and age-related macular degeneration. *Vision Res.* **50**, 652-664.

Canto-Soler, V., Flores-Bellver, M. and Vergara, M. N. (2016). Stem cell sources and their potential for the treatment of retinal degenerations. *Invest. Ophthalmol. Vis. Sci.* **57**, ORSFd1-O9.

Fatehullah, A., Tan, S. H. and Barker, N. (2016). Organoids as an in vitro model of human development and disease. *Nat. Cell Biol.* **18**, 246-254.

Hollyfield, J. G., Bonilha, V. L., Rayborn, M. E., Yang, X., Shadrach, K. G., Lu, L., Ufret, R. L., Salomon, R. G. and Perez, V. L. (2008). Oxidative damage-induced inflammation initiates age-related macular degeneration. *Nat. Med.* **14**, 194-198.

Hynds, R. E. and Giangreco, A. (2013). Concise review: the relevance of human stem cell-derived organoid models for epithelial translational medicine. *Stem Cells* **31**, 417-422.

Inglese, J., Johnson, R. L., Simeonov, A., Xia, M., Zheng, W., Austin, C. P. and Auld, D. S. (2007). High-throughput screening assays for the identification of chemical probes. *Nat. Chem. Biol.* **3**, 466-479.

Jarrett, S. G. and Boulton, M. E. (2012). Consequences of oxidative stress in age-related macular degeneration. *Mol. Aspects Med.* **33**, 399-417.
Johnson, J. Z. and Hockemeyer, D. (2015). Human stem cell-based disease modeling: prospects and challenges. *Curr. Opin. Cell Biol.* **37**, 84-90.
Kowluru, R. A. and Chan, P. S. (2007). Oxidative stress and diabetic retinopathy. *Exp. Diabetes Res.* **2007**, 43603.
Kuse, Y., Ogawa, K., Tsuruma, K., Shimazawa, M. and Hara, H. (2014). Damage of photoreceptor-derived cells in culture induced by light emitting diode-derived blue light. *Sci. Rep.* **4**, 5223.
Lichtman, J. W. and Conchello, J.-A. (2005). Fluorescence microscopy. *Nat. Methods* **2**, 910-919.
Little, M. H. (2016). Closing the circle: from organoids back to development. *Development* **143**, 905-906.
Masuda, T., Shimazawa, M. and Hara, H. (2017). Retinal diseases associated with oxidative stress and the effects of a free radical scavenger (Edaravone). *Oxid. Med. Cell Longev.* **2017**, 9208489.
Michael, S., Auld, D., Klumpp, C., Jadhav, A., Zheng, W., Thorne, N., Austin, C. P., Inglese, J. and Simeonov, A. (2008). A robotic platform for quantitative high-throughput screening. *Assay Drug Dev. Technol.* **6**, 637-657.
Nishimura, Y., Hara, H., Kondo, M., Hong, S. and Matsugi, T. (2017). Oxidative stress in retinal diseases. *Oxid. Med. Cell Longev.* **2017**, 4076518.
Nita, M. and Grzybowski, A. (2016). Smoking and eye pathologies. A systemic review. Part I. Anterior eye segment pathologies. *Curr. Pharm. Des.* **23**, 629-638.
Panfoli, I., Calzia, D., Ravera, S., Candiano, G., Bachi, A., Bianchini, P. and Diaspro, A. (2009). A new protocol for live imaging of mammalian retina ex vivo by confocal laser scanning microscopy. *Protocol Exchange*, doi:10.1038/nprot.2009.101.
Paul, S. M., Mytelka, D. S., Dunwiddie, C. T., Persinger, C. C., Munos, B. H., Lindborg, S. R. and Schacht, A. L. (2010). How to improve R&D productivity: the pharmaceutical industry's grand challenge. *Nat. Rev. Drug Discov.* **9**, 203-214.
Pearson, R. A., Gonzalez-Cordero, A., West, E. L., Ribeiro, J. R., Aghaizu, N., Goh, D., Sampson, R. D., Georgiadis, A., Waldron, P. V., Duran, Y. et al. (2016). Donor and host photoreceptors engage in material transfer following transplantation of post-mitotic photoreceptor precursors. *Nat. Commun.* **7**, 13029.
Rajendram, R., Saraswathy, S. and Rao, N. A. (2007). Photoreceptor mitochondrial oxidative stress in early experimental autoimmune uveoretinitis. *Br. J. Ophthalmol.* **91**, 531-537.
Ranga, A., Gjorevski, N. and Lutolf, M. P. (2014). Drug discovery through stem cell-based organoid models. *Adv. Drug Deliv. Rev.* **69-70**, 19-28.
Roehlecke, C., Schumann, U., Ader, M., Knels, L. and Funk, R. H. (2011). Influence of blue light on photoreceptors in a live retinal explant system. *Mol. Vis.* **17**, 876-884.
Wahlin, K. J., Maruotti, J. A., Sripathi, S. R., Ball, J., Angueyra, J. M., Kim, C., Grebe, R., Li, W., Jones, B. W. and Zack, D. J. (2017). Photoreceptor outer segment-like structures in long-term 3D retinas from human pluripotent stem cells. *Sci. Rep.* **7**, 766.
Walker, S. L., Ariga, J., Mathias, J. R., Coothankandaswamy, V., Xie, X., Distel, M., Köster, R. W., Parsons, M. J., Bhalla, K. N., Saxena, M. T. et al. (2012). Automated reporter quantification in vivo: high-throughput screening method for reporter-based assays in zebrafish. *PLoS ONE* **7**, e29916.
Wang, G., Rajpurohit, S. K., Delaspre, F., Walker, S. L., White, D. T., Ceasrine, A., Kuruvilla, R., Li, R. J., Shim, J. S., Liu, J. O. et al. (2015). First quantitative high-throughput screen in zebrafish identifies novel pathways for increasing pancreatic beta-cell mass. *Elife* 4, e08261.
White, D. T., Eroglu, A. U., Wang, G., Zhang, L., Sengupta, S., Ding, D., Rajpurohit, S. K., Walker, S. L., Ji, H., Qian, J. et al. (2016). ARQiv-HTS, a versatile whole-organism screening platform enabling in vivo drug discovery at high-throughput rates. *Nat. Protoc.* **11**, 2432-2453.
Wright, L. S., Phillips, M. J., Pinilla, I., Hei, D. and Gamm, D. M. (2014). Induced pluripotent stem cells as custom therapeutics for retinal repair: progress and rationale. *Exp. Eye Res.* **123**, 161-172.
Xinaris, C., Brizi, V. and Remuzzi, G. (2015). Organoid models and applications in biomedical research. *Nephron* **130**, 191-199.
Yin, X., Mead, B. E., Safaee, H., Langer, R., Karp, J. M. and Levy, O. (2016). Engineering stem cell organoids. *Cell Stem Cell* **18**, 25-38.
Zhang, X. D. (2008). Novel analytic criteria and effective plate designs for quality control in genome-scale RNAi screens. *J. Biomol. Screen.* **13**, 363-377.
Zhang, X. D. (2011). Illustration of SSMD, z score, SSMD*, z* score, and t statistic for hit selection in RNAi high-throughput screens. *J. Biomol. Screen.* **16**, 775-785.
Zhong, X., Gutierrez, C., Xue, T., Hampton, C., Vergara, M. N., Cao, L. H., Peters, A., Park, T. S., Zambidis, E. T., Meyer, J. S. et al. (2014). Generation of three-dimensional retinal tissue with functional photoreceptors from human iPSCs. *Nat. Commun.* **5**, 4047.

Table S1. Recommended microplate reader parameters

Parameter	Optimized settings	Reason
Plate type	Greiner 96 well, black	Black plates reduce background and fluorescence crosstalk, improves sensitivity. (Z'=0.19 for black U-bottom vs. Z'=0.00 for clear U-bottom plates)
Well shape	V-bottom	Retinal organoids naturally self-center. Simplifies fluorescent plate reads. (Z'=0.33 for black V-bottom vs. Z'=0.19 for black U-bottom plates)
Read mode	Top read	Allows Z-dimensional focus and the use of black v-bottom plates.
Volume	340 µl	Fills well completely, no meniscus.
Flash mode	1 (400 Hz)	A high flash mode increases sensitivity. However if sample viability were a concern (especially if using lower media volumes), a lower flash mode (100 Hz) can be used instead. (Z'=0.33 for 400Hz vs. Z'=0.32 for 100 Hz).
# of flashes	20	Lower flash numbers increase speed (throughput). Higher flash numbers improve accuracy. (See Table S2)

Assay parameters were determined by scanning transgenic GFP-expressing retinal organoids and wild type controls (n=6/condition).

Table S2. Estimated throughput performance

# of flashes	2	5	10	20	50	
Scan time per well	0.1875	0.1979	0.2187	0.2395	0.3229	sec
Scan time per plate	18	19	21	23	31	sec
Estimated daily capacity	2,618	2,541	2,400	2,273	1,878	plates
Estimated daily capacity	251,345	243,952	230,400	218,273	180,313	Individual retinal organoids
SSMD*	>> 2	>> 2	>> 2	>> 2	>> 2	
Z' factor (for n=6)	0.30	0.31	0.32	0.33	0.33	

Estimated daily capacity was calculated adding 15 seconds per 96 well plate to account for handling time between plates. SSMD*: robust SSMD (strictly standardized mean difference).

Table S3. Analytic metrics for evaluating assay quality

Parameter	Formula	Interpretation	HTS compatible values
Signal to background ratio	$S{:}B = \frac{\mu_p}{\mu_n}$	Measures the sensitivity of the assay for signal detection; normally calculated using controls.	>2-fold
Coefficient of variation	$\%CV = \frac{\sigma}{\mu} \times 100$	Represents intra-assay precision or repeatability.	<15%
SSMD*	$\hat{\beta} = \frac{\tilde{X}_p - \tilde{X}_n}{1.4826\sqrt{(\tilde{s}_p)^2 + (\tilde{s}_n)^2}}$	Proposed as a preferred measure of HTS assay quality due to its robustness	$\hat{\beta}$ ≥ 2: excellent quality 2 > $\hat{\beta}$ ≥1: good quality 1 > $\hat{\beta}$ ≥ 0.5: acceptable quality $\hat{\beta}$ < 0.5: poor quality
Z' factor	$Z' = 1 - \frac{(3\,\sigma_p + 3\sigma_n)}{\lvert\mu_p - \mu_n\rvert}$	An accepted, more stringent measure of HTS assay quality. Z' is used in the absence of library compounds to optimize an assay prior to screen.	> 0.5: excellent quality 0 to 0.5: acceptable quality = 0: for "yes/no" type of assay < 0: should be improved

"*p*" and "*n*" correspond to the values of positive and negative controls respectively. μ: mean; σ: standard deviation; SSMD*: robust SSMD (strictly standardized mean difference); $\tilde{X}$: sample median; $\tilde{s}$: sample median absolute deviation. (Described in detail in Inglese at el., 2007; White et al., 2016; and Zhang, 2008, 2011).

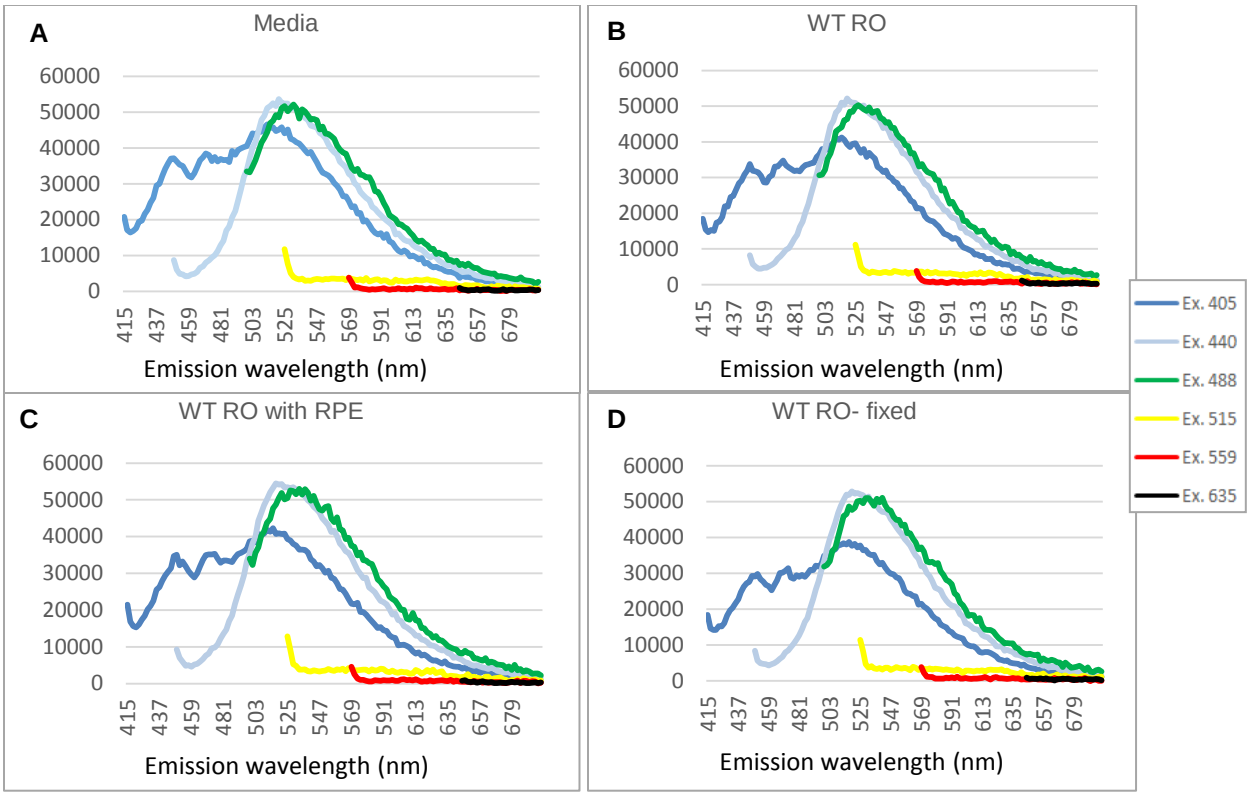

Figure S1. Background fluorescence profiles. (A-D) Graphs show fluorescence emission profiles for common excitation wavelengths (see inset). Fluorescence intensity scans were performed on clear media (A); live, not labeled, wild type retinal organoids (RO, B); retinal organoids with small amounts of RPE attached to the tip (C); and retinal organoids fixed with 4% paraformaldehyde for 10 minutes (D). Curves represent average fluorescence profiles of 5 independent ROs per condition.

A

Fluorophore	Excitation (nm)	Emission (nm)
Hoechst	350/5	450/5
GFP	485/5	510/15
Calcein	492/5	513/5
YFP	514/5	534/10
DiI	551/5	569/5
Bodipy TR	592/5	624/5
Sytox green	504/5	526/5

B

DiI

Ex\Em	560	562	564	566	568	570	572	574	576	578	580
535	670	755	898	782	805	841	931	982	859	702	859
537	777	831	809	974	1016	1028	812	867	716	762	704
539	688	774	685	914	899	858	906	829	823	842	801
541	804	750	972	978	912	1055	924	924	897	837	856
543	1040	895	952	1041	957	1004	971	943	955	896	879
545	851	888	829	1029	941	1078	1061	1082	1033	866	824
547	957	1154	1041	994	1040	1021	1062	1131	1019	919	979
549	1197	1044	1223	1263	1338	1161	1052	1090	1076	978	847
551	1522	1286	1332	1071	1237	1387	1089	1085	1157	807	963
553	3235	1825	1770	1323	1237	1265	1514	1318	1102	1382	1033
555	420898	3905	1999	1582	1512	1513	1412	1426	1141	1085	1060
557	OVER	305033	3443	2269	1726	1412	1373	1142	1152	1046	1049
559	OVER	OVER	61654	3393	1944	1708	1341	1129	1267	1015	1015

Figure S2. Optimized excitation and emission wavelengths. (A) Table shows the optimal excitation and emission wavelengths identified by performing 3D fluorescence scans (i.e. scans spanning a range of excitation and emission wavelengths) on transgenic retinal organoids (GFP and YFP), or retinal organoids stained with different fluorescent dyes (Hoechst, calcein, DiI, Bodipy TR, Sytox green). Live organoids were used for this experiment, with the exception of Sytox green, which was used on fixed organoids. Results are expressed as "wavelength/bandwidth". (B) Example of a 3D scan performed for one of the conditions (DiI staining). Heat map is a visual representation used to aid in the determination of optimal parameters. Lowest wavelength values (blue) provide decreased sensitivity, whereas highest values (red) constitute an artifact from the overlap of the excitation an emission spectral curves. Box illustrates the wavelengths that were chosen for their sensitivity performance among the mid ranges of the matrix (green color set at the 50th percentile).

SUPPLEMENTARY METHODS

Generation of transgenic hiPSC lines

The human episomal CB-iPSC6.2 line (A18945, ThermoFisher Scientific; Burridge et al., 2011) was maintained on Matrigel (growth-factor-reduced; BD Biosciences)-coated plates with mTeSR1 medium (Stemcell Technologies). Transgenic cell lines were generated by electroporation with the Neon Transfection System (Invitrogen) according to manufacturer instructions as described in Ranganathan et al., 2014. The following plasmid DNAs were used: i) CRISPR/Cas9-mediated constitutively expressed GFP hiPSC line: 1µg of AAV-CAGGS-EGFP donor vector (Addgene # 22212, gift from Rudolf Jaenisch; Hockemeyer et al., 2009); 0.6 µg of pCas9_GFP (Addgene # 44719, gift from Kiran Musunuru); and 0.3 µg of gRNA_AAVS1-T2 (Addgene # 41818, gift from George Church; Mali et al., 2013); ii) PiggyBac transposon-mediated constitutively expressed membrane YFP hiPSC line: 1 µg of PB-myr-tagged YFP donor vector and 0.3 µg of PB-HA transposase expression vector (Wellcome Trust Sanger Institute; Cadiñanos et al., 2007).

Briefly, cells were pre-treated with 5 µM blebbistatin for 24h to increase cell viability, followed by treatment with Accutase (Stemcell Technologies) for 5min, dissociation into single cells, centrifugation at 80 x g for 5 min. for pellet formation and incubation on ice for 15 min. The corresponding plasmids for each transgenic cell line were combined in R buffer, resuspended in the plasmid cocktail and electroporated with a 10 µl tip-type and the following parameters: 1,300 V; 20 ms pulse length; 1 pulse. Cells were then gently resuspended into 1ml of mTeSR1 plus 5µM blebbistatin, incubated at room temperature for 20 min and plated onto Matrigel-coated 35mm TC treated dishes containing mTeSR1 and 5 µM blebbistatin. Finally, cells were incubated at room temperature for 20 min and cultured thereafter in 37 C and 5% CO2. After 5 days, stable clonal sublines were manually selected with a Leica MZ-16F fluorescence stereomicroscope.

Media and dye solutions for staining of retinal organoids

Fluorescent staining and scanning of retinal organoids was performed in clear retinal differentiation medium (cRDM) containing 60% DMEM/F12 no phenol red (cat# 21041-025), and 40% FluoroBrite DMEM (cat# A18967-01), supplemented with 1x B27 (cat# 12587-010), 0.4x Glutamax (cat# 35050-079), 1x MEM-Non essential amino acids (cat# 11140-050), and 1x antibiotic-antimycotic (cat# 15240-062), all from Thermo Fisher Scientific. Solutions of the corresponding dyes were prepared in cRDM as follows: Hoechst 33342 (cat# H3570), 2.5 µl/ml; Calcein AM 4mM stock solution in DMSO (cat# C34852), 2.75 µl/ml ; Vybrant CM-DiI (cat# V-22888), 5 µl/ml; and Bodipy TR (cat# C34556), 20 µl/ml; Sytox green 5 mM (cat# S7020), 2 µl/ml (all from Thermo Fisher Scientific). Staining was performed as described in Methods. Long-term suspension culture media for aged retinal organoids consists of DMEM/F12 -Glutamax (cat#10565018, ThermoFisher Scientific) supplemented with 1% N2 (cat# 17502048, ThermoFisher Scientific), 1x MEM-Non essential amino acids, 1% antibiotic–antimycotic, 100 µM Taurine (cat# T0625, Sigma-Aldrich), and 10% fetal bovine serum (cat# S11150, Atlanta Biologicals), as described in Zhong et al., 2014.

Whole-mount immunofluorescence

Retinal organoids were fixed in 4% paraformaldehyde for 10 min and rinsed 3X in PBS, followed by 3X 20 min washes in PBST (0.25% Triton X-100 in PBS) with rocking.

For Otx2 immunofluorescence organoids were blocked in 10% NGS (normal goat serum), 0.25% PBST, overnight at room temperature. They were then washed 3X 30 min in 0.25% PBST, and 3X 30 min in PBS, followed by incubation in rabbit-anti-Otx2 antibody (cat# AB9566; ThermoFisher Scientific) diluted 1/500 in 2% NGS, 0.25% PBST for 2 days at room temp with rocking. Subsequently, organoids were rinsed 3X 30 min in 0.25% PBST, and 3X 30 min in PBS, followed by incubation with secondary antibody: goat-anti-mouse Alexafluor 514 (cat# A-31558; ThermoFisher Scientific) , diluted 1/500, in 2%NGS, 0.25% PBST, for 2 days at room temp with rocking. Finally, they were washed 3X 30 min in

0.25% PBST, and 3X 30 min in PBS. For size normalization organoids were counterstained by incubation with Bodipy TR, 20 µl/ml at 37°C for 90 min, followed by 3 washes in cRDM, and plated in black v-bottom 96-well plates for scanning.

For Pou4f2 immunofluorescence organoids were blocked in 10% NDS (normal donkey serum), 0.25% PBST, overnight at 4°C. They were then washed 3X 30 min in 0.25% PBST, and 3X 30 min in PBS, followed by incubation in goat-anti-Brn3b(Pou4f2) antibody (Santa Cruz Biotechnologies, cat# SC-6026x) diluted 1/1000 in 2% NDS, 0.25% PBST for 3 days at 4°C with rocking. Subsequently, organoids were rinsed 3X 30 min in 0.25% PBST, and 3X 30 min in PBS, followed by incubation with secondary antibody: donkey-anti-goat-Alexafluor 546 (ThermoFisher Scientific, cat# A-11056), diluted 1/500, in 2%NDS, 0.25% PBST, for 3 days at 4°C with rocking. Finally, they were washed 3X 30 min in 0.25% PBST, and 3X 30 min in PBS. For size normalization organoids were counterstained by incubation with Sytox green, 10 µM at 37°C for 90 min, followed by 3 washes in cRDM, and plated in black v-bottom 96-well plates for scanning.

Immunofluorescence on cryosections

Retinal organoids were fixed in 4% paraformaldehyde for 10 min and rinsed 3X in PBS, followed by sucrose gradient and embedding in a 1:1 mixture of 25% sucrose:OCT. 12 µm thick sections were obtained using a cryostat, and slides were incubated at room temperature for 60 minutes, followed by PBS wash and blocking in 10% NGS, 0.25% PBST for 1 hour. Slides were then incubated overnight at 4°C in anti-recoverin antibody (cat# AB5585, Millipore- ThermoFisher Scientific) diluted 1/500 in 2% NGS, 0.25% PBST. After 3X 10 min. washes in PBS, slides were incubated in secondary antibody: goat-anti-rabbit Alexafluor 546 (cat# A-11035; ThermoFisher Scientific), diluted 1/500, in 2%NGS, 0.25% PBST, for 2 hrs. at room temp. Finally, they were washed 3X 10 min in PBS and incubated for 5 min. in DAPI (cat# D1306; ThermoFisher Scientific) for nuclear counterstaining. Imaging was performed using a Zeiss LSM 510 confocal microscope.

Eqn. S1. Size normalization

$$Norm.X_a = \frac{X_a * \overline{Y}}{Y_a}$$

$Norm.X_a$: Normalized fluorescence intensity value of fluorophore X for organoid a.
X_a: Fluorescence intensity value of fluorophore X for organoid a.
Y_a: Fluorescence intensity value of global fluorophore Y (normalizer) for organoid a.
$\overline{Y}$: Mean of fluorescence intensity values for fluorophore Y.

SUPPLEMENTARY REFERENCES

Hockemeyer, D., Soldner, F., Beard, C., Gao, Q., Mitalipova, M., Dekelver, R.C., Katibah, G.E., Amora, R., Boydston, E.A., Zeitler, B., Meng, X., Miller, J.C., Zhang, L., Rebar, E.J., Gregory, P.D., Urnov, F.D., Jaenisch, R. (2009). Efficient targeting of expressed and silent genes in human ESCs and iPSCs using zinc-finger nucleases. *Nat. Biotechnol.* **27**, 851-7.

Mali, P., Yang, L., Esvelt, K.M., Aach, J., Guell, M., Dicarlo, J.E., Norville, J.E., Church, G.M. (2013). RNA-Guided Human Genome Engineering via Cas9. *Science* **339**, 823-6.

Ranganathan, V., Wahlin, K., Maruotti, J., Zack, D.J. (2014). Expansion of the CRISPR–Cas9 genome targeting space through the use of H1 promoter-expressed guide RNAs. *Nat. Commun*. **5**, 4516.

Cadiñanos, J. and Bradley, A. (2007). Generation of an inducible and optimized *piggyBac* transposon system. *Nucleic Acids Res.* **35,** e87.